Phase separation, crystallization and polyamorphism in the Y_2O_3–Al_2O_3 system

2008 J. Phys.: Condens. Matter 20 205103

(http://iopscience.iop.org/0953-8984/20/20/205103)

J. Phys.: Condens. Matter **20** (2008) 205103 (9pp) doi:10.1088/0953-8984/20/20/205103

Phase separation, crystallization and polyamorphism in the Y_2O_3–Al_2O_3 system

Lawrie B Skinner[1], Adrian C Barnes[1], Philip S Salmon[2] and Wilson A Crichton[3]

[1] H H Wills Physics Laboratory, Royal Fort, Tyndall Avenue, Bristol BS8 1TL, UK
[2] Department of Physics, University of Bath, Bath BA2 7AY, UK
[3] European Synchrotron Radiation Facility, 6 rue Jules Horowitz, BP 220, Grenoble Cedex, F-38043, France

E-mail: a.c.barnes@bristol.ac.uk

Received 14 February 2008
Published 17 April 2008
Online at stacks.iop.org/JPhysCM/20/205103

Abstract

A detailed study of glass formation from aerodynamically levitated liquids in the $(Y_2O_3)_x(Al_2O_3)_{1-x}$ system for the composition range $0.21 \leqslant x \leqslant 0.41$ was undertaken by using pyrometric, optical imaging and x-ray diffraction methods. Homogeneous and clear single-phase glasses were produced over the composition range $0.27 \lesssim x \lesssim 0.33$. For Y_2O_3-rich compositions ($0.33 \lesssim x \leqslant 0.375$), cloudy materials were produced which contain inclusions of crystalline yttrium aluminium garnet (YAG) of diameter up to 40 μm in a glassy matrix. For Y_2O_3-poor compositions around $x = 0.24$, cloudy materials were also produced, but it was not possible to deduce whether this resulted from (i) sub-micron inclusions of a nano-crystalline or glassy material in a glassy matrix or (ii) a glass formed by spinodal decomposition. For $x = 0.21$, however, the sample cloudiness results from crystallization into at least two phases comprising yttrium aluminium perovskite and alumina. The associated pyrometric cooling curve shows slow recalescence events with a continuous and slow evolution of excess heat which contrasts with the sharp recalescence events observed for the crystallization of YAG at compositions near $x = 0.375$. The materials that are the most likely candidates for demonstrating homogeneous nucleation of a second liquid phase occur around $x = 0.25$, which corresponds to the limit for formation of a continuous random network of corner-shared AlO_4 tetrahedra.

(Some figures in this article are in colour only in the electronic version)

1. Introduction

The $(Y_2O_3)_x(Al_2O_3)_{1-x}$ (yttria–alumina) system has attracted attention in recent years following the report by Aasland and McMillan (1994) on the glasses formed by bulk quenching liquids in the composition range $0.24 \leqslant x \leqslant 0.32$. In this work liquid $(Y_2O_3)_x(Al_2O_3)_{1-x}$ samples were held in the iridium wire furnace of a hot-stage microscope and were quenched at different rates by rapidly reducing the furnace power and controlling the flow of nitrogen gas. The samples thus produced were reported to comprise glassy inclusions in a glassy matrix of higher density, and evidence from microprobe analysis led to the conclusion that the matrix and inclusions were of identical compositions and therefore correspond to the high-density amorphous (HDA) and low-density amorphous (LDA) forms of the same material. Since these inclusions began to form in the supercooled state, it was suggested that the observed behaviour is evidence for the existence of a liquid–liquid phase transition (Mishima and Stanley 1998) in the supercooled state. A recent summary of polyamorphism in the $(Y_2O_3)_x(Al_2O_3)_{1-x}$ system, which includes a description of work on mechanical separation of the LDA and HDA phases, is given elsewhere (McMillan *et al* 2003).

However, in a separate study by Nagashio and Kuribayashi (2002), glassy samples of $(Y_2O_3)_x(Al_2O_3)_{1-x}$ were produced by using a contactless aero-acoustic levitation and laser heating system. The levitated samples were quenched in the surrounding dry oxygen gas atmosphere after the laser was switched off or, to increase the cooling rate, they were splat quenched between a pair of stainless-steel or copper

anvils. The samples were studied optically, by differential thermal analysis and by micro-focus x-ray diffraction, and very different behaviour was observed to that reported by Aasland and McMillan (1994). For gas quenched samples with $0.25 \leqslant x < 0.325$ single-phase glasses could only be obtained, and for similarly quenched samples with $0.325 \leqslant x \leqslant 0.375$ small yttrium aluminium garnet ($Y_3Al_5O_{12}$ garnet or YAG) crystalline inclusions were found in a bulk glassy matrix. By very rapid quenching using anvils, it was possible to produce single-phase bulk glasses over the entire composition range $0.25 \leqslant x \leqslant 0.375$. It was concluded that there is no evidence for polyamorphic samples, in direct contrast and in contradiction to the behaviour observed by McMillan *et al* (2003).

In the present work we have studied the properties of liquid and glassy $(Y_2O_3)_x(Al_2O_3)_{1-x}$ for the composition range $0.21 \leqslant x \leqslant 0.41$ by using an aerodynamic levitation and laser heating system to melt and quench the samples. In particular, we have monitored crystallization and glass formation by fast pyrometric studies of the liquid as it is quenched. In addition, we have examined the structure of the quenched materials by optical microscopy and high-energy x-ray diffraction.

2. Experimental method

An aerodynamic levitation and laser heating system, supplied by Containerless Research Inc. (Evanston, IL, USA), was used to study $(Y_2O_3)_x(Al_2O_3)_{1-x}$ liquids and glasses over the composition range $0.21 \leqslant x \leqslant 0.41$. The apparatus was modified to include a fast sampling (100 Hz) pyrometer (model ISQ5 from IMPAC, Frankfurt-am-Main, Germany) used in single-wavelength (0.9 μm) mode and direct computer control of the CO_2 laser output. This system allows the sample temperature to be monitored synchronously with the applied laser power. Since the emissivity of a sample changes on crystallization or vitrification, we have not applied an emissivity correction to the recorded temperature. This leads to an underestimate of the sample temperature by approximately 30 °C, as evaluated by using an emissivity value of 0.92 for molten yttria–alumina (Nordine *et al* 2000). Controlled reduction of the applied laser power allows the sample to be cooled at well defined rates. In the absence of any changes in emissivity or phase transitions, the sample temperature decreases monotonically with a broadly black-body behaviour. Phase transitions such as nucleation and growth give rise to an evolution of excess heat from the sample and lead to a characteristic rise and decay of the temperature over and above that predicted by black-body cooling.

The samples were prepared from 99.99% purity metal oxides (Al_2O_3 and Y_2O_3) purchased from Sigma-Aldrich and RE acton, respectively. Before use, all of the metal oxide powders were heated in air to 800 °C in a muffle furnace for at least 2 h in order to remove any adsorbed water. To obtain optimum control over the sample composition, the pure oxides were first formed into small spheres on a copper laser hearth. A sample of the required composition was then obtained by fusing weight-matched beads on the copper hearth. Final mixing and equilibration of the sample took place *in situ* on the aerodynamic levitator. In this way the error in the sample composition, δx, could be estimated by comparing the mass of the final sample to the masses of the starting spheres, and a value $\delta x < 0.005$ was obtained. The levitated samples were heated with the laser beam impinging directly onto the top. Cooling by the levitation gas results in a temperature gradient of approximately 50 °C between the top and bottom of the sample.

Glasses were produced from liquids levitated on a pure argon (99.999%) gas stream by first heating the samples to a temperature at least 200 °C above the measured melting temperature, maintaining this temperature for ≃60 s, and then controlling the rate at which the laser power was reduced. This procedure was used in order to avoid errors associated with the variation in quoted values for the melting temperature (Caslavsky and Viechnicki 1980, Cockayne 1985) and to exceed the critical temperature needed to ensure that any remnants of YAG seeding crystals are removed from the melt (Gervais *et al* 1992, 1997). For a sample with a typical mass of 25 mg, the fastest quench rate was obtained by instantaneously cutting the laser power to zero, and this corresponds to a cooling rate of ≃300 °C s^{-1} at 1200 °C. Slower quench rates could be produced by using a computer-controlled linear decrease of the laser power. In all cases the laser power and pyrometric temperature were recorded synchronously.

Quenched spheres of $(Y_2O_3)_x(Al_2O_3)_{1-x}$ were obtained over the composition range $0.21 \leqslant x \leqslant 0.41$. High-energy x-ray diffraction experiments with an incident wavelength of 0.173 Å (the rhenium K edge) were undertaken using the ID27 diffractometer at the European Synchrotron Radiation Facility (ESRF) with a charge-coupled device (CCD) detector. The measurements were made in transmission mode on polished disks of ≃1 mm thickness prepared from the quenched spheres. Data of high statistical precision were accumulated over a range $1.35 \leqslant Q \leqslant 23$ Å^{-1}, where Q denotes the scattering vector (Fischer *et al* 2006).

For the optical microscopy experiments the samples were polished into optically flat discs of approximately 2.5 mm diameter and thickness less than 1 mm by using a fine diamond polisher. Optical images were recorded by using a phase contrast microscope (Zeiss-Autophot) with both crossed and uncrossed polarizers and parallel light.

3. Results

Figure 1 shows photographs of ≃2.3–2.5 mm diameter $(Y_2O_3)_x(Al_2O_3)_{1-x}$ samples formed from spherical liquid drops of mass ≃25 mg by quenching at a rate of ≃300 °C s^{-1} at 1200 °C after instantaneously cutting the laser power. At the yttria-rich extreme of the composition range ($x = 0.41$) the recovered sample was non-spherical in appearance and consisted of small crystals. At the alumina-rich extreme of the composition range ($x = 0.21$) the recovered sample appeared off-white and opaque but remained spherical with a smooth surface. The samples with compositions $x = 0.27$ and 0.33 remained spherical and were optically transparent with a typical glassy appearance. The samples with compositions

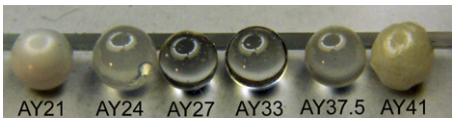

Figure 1. Photographs of ≃2.3–2.5 mm diameter solid samples of $(Y_2O_3)_x(Al_2O_3)_{1-x}$ produced on the aerodynamic levitator. The labels correspond to the following compositions: AY21 ($x = 0.21$), AY24 ($x = 0.24$), AY27 ($x = 0.27$), AY33 ($x = 0.33$), AY37.5 ($x = 0.375$) and AY41 ($x = 0.41$).

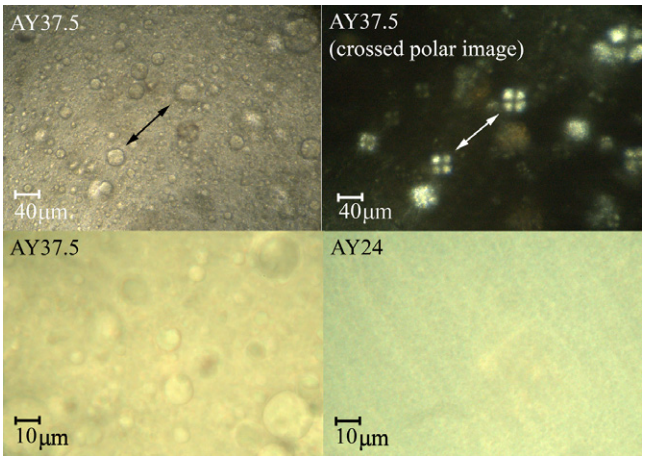

Figure 2. Optical images of sections of the spheres labelled AY24 and AY37.5 in figure 1. The upper row corresponds to the YAG composition $x = 0.375$ and shows an image of the inclusions as viewed through uncrossed and crossed polarizers. The dark crosses viewed through crossed polarizers (some of which are indicated by the arrows) are characteristic of the birefringence for small crystalline spherulites. The lower row compares magnified images for the $x = 0.375$ and 0.24 samples. It is notable that the $x = 0.24$ sample shows no micron or larger sized inclusions.

$x = 0.24$ and 0.375 (YAG) appeared spherical and glassy but had a distinct 'cloudy' (turbid) appearance, which suggests the existence of two separate phases. The density of the YAG composition sample was 4.1 ± 0.1 g cm^{-3}, as determined by Archimedes principle using toluene. This compares with a density for crystalline YAG of 4.56 g cm^{-3} obtained from the unit cell data of Euler and Bruce (1965). The density of the other samples decreases steadily with x and reaches a value of 3.8 ± 0.1 g cm^{-3} at $x \simeq 0.21$.

3.1. Optical microscopy

The polished sample discs were examined under an optical microscope. For the clear samples, in the centre of the composition range, no texture in the material was observed, which suggests a single homogeneous phase. Figure 2 shows the optical micrographs of the cloudy samples with $x = 0.24$ and 0.375. Although macroscopically similar in appearance, a clear difference is noticed between the two compositions. For the $x = 0.375$ sample, spherical inclusions of diameter up to ≃40 μm could be clearly observed and, under crossed polarizers, these inclusions showed distinct 'Maltese cross' birefringence, which is indicative of crystalline spherulites

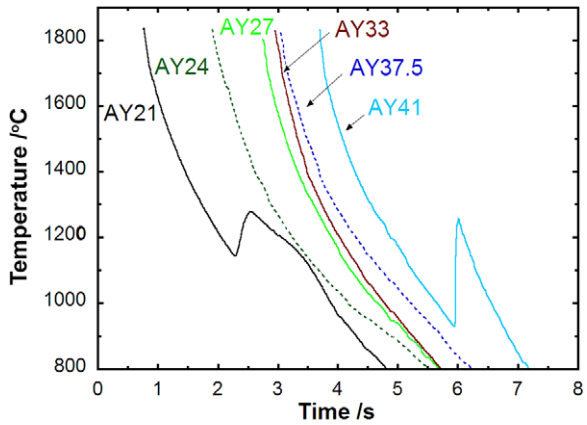

Figure 3. Pyrometer traces for the $(Y_2O_3)_x(Al_2O_3)_{1-x}$ samples when quenched rapidly (≃300 °C s^{-1} at 1200 °C) by instantaneously cutting the laser power. The curves are annotated according to the labels shown in figure 1. The abscissa (time) for each cooling curve has an arbitrary origin.

(Morse and Donnay 1932, 1936). In contrast, for the $x = 0.24$ sample, no large inclusions were observed and the image was uniform while maintaining its cloudy appearance. This indicates that the inclusions, if they exist, are sub-micron in size.

3.2. Pyrometric measurements of sample quenching

Figure 3 shows examples of the sample temperature, measured as a function of time, when the laser power was instantaneously cut for the materials that were studied over the composition range $0.21 \leqslant x \leqslant 0.41$. This corresponds to a quench rate of ≃300 °C s^{-1} at 1200 °C. The cooling curves for samples with composition $0.24 \leqslant x \leqslant 0.375$ are characterized by a monotonically decreasing temperature, which is consistent with black-body-like behaviour. The cooling curves for the other samples showed a recalescence event which is characterized by a brief and rapid rise in the sample temperature with time. When the heat–quench cycle was repeated, identical and reproducible behaviour was found for all compositions except $x = 0.41$. In this case, the lowest temperature achieved before the onset of crystallization was ≃900 °C, which therefore corresponds to the highest degree of supercooling, and the sample always recalesced but showed variations in the post-recalescence behaviour. A variation in the cooling behaviour of the $x = 0.41$ sample was also found when slower quench rates were used (see figure 4) and this is consistent with the rapid nucleation and growth of large crystals at slightly different times in different parts of the cooling sphere. The recalescence temperature was found to increase as the quench rate decreased. For the $x = 0.21$ sample, a strong recalescence feature was always observed, but the form of this recalescence was notably different to the case of $x = 0.41$, i.e. the sample always started to recalesce at a higher temperature ($T \simeq 1200$ °C) and the rise in temperature was noticeably slower. In addition, heat appeared to evolve continuously from the $x = 0.21$ sample for approximately 1.5 s after the recalescence event before the cooling curve resumed

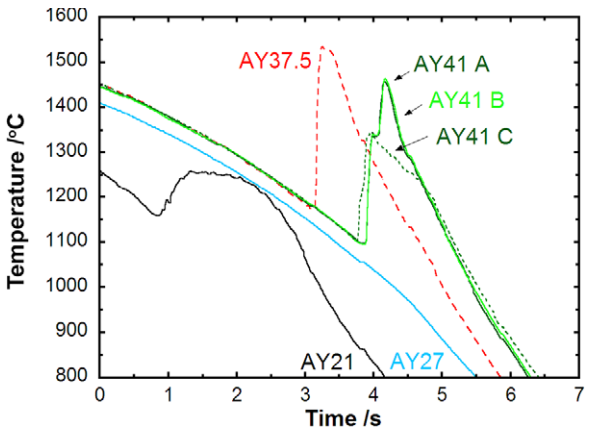

Figure 4. Pyrometer traces for several of the $(Y_2O_3)_x(Al_2O_3)_{1-x}$ samples when cooled slowly ($\simeq$100 °C s^{-1} at 1200 °C) under laser control. The curves marked AY41A, AY41B and AY41C all correspond to the same sample but to the cooling stages of different heating/cooling cycles. The abscissa (time) for each cooling curve has an arbitrary origin.

a characteristic black-body shape. Again, the recalescence temperature increased as the quench rate was decreased.

3.3. High-energy x-ray diffraction

Figure 5 shows the x-ray diffraction patterns measured using the ID27 diffractometer for rapidly quenched samples of diameter $\simeq$2.3–2.5 mm with compositions $x = 0.21$, 0.24, 0.30 and 0.375. The powder diffraction patterns for crystalline YAG ($x = 0.375$) (Prince 1957, Fletcher *et al* 1996) and yttrium aluminium perovskite (YAP corresponding to $x = 0.50$) (Ross *et al* 2004) are also shown. The cloudy sample at the YAG composition is a glass-ceramic with partly amorphous and partly crystalline components. Comparison with the diffraction pattern for crystalline YAG shows that the small inclusions observed by optical microscopy (see figure 2) correspond to spherical YAG crystals embedded in a glassy matrix. Separate diffraction measurements (not illustrated) of YAG composition samples quenched at different rates show that the Bragg peak intensity increases with cloudiness. In comparison, the diffraction pattern for the clear $x = 0.30$ sample shows no evidence of Bragg diffraction and is consistent with a single glassy phase. At first sight, the diffraction pattern for the cloudy $x = 0.24$ sample also appears to be characteristic of a pure glass. For example, there is no strong Bragg peak on the high-Q side of the principle diffraction peak at $\simeq$2.2 Å^{-1}, as observed in the diffraction pattern for the $x = 0.375$ sample, and no sharp Bragg peaks appear elsewhere. However, when compared to the $x = 0.3$ sample, the diffraction pattern appears more structured, especially with regard to the bumps observed at Q-values of $\sim$3.1 and $\sim$4.5 Å^{-1}. These do not appear to correspond to any of the Bragg peaks for YAG or YAP, and it is possible that they result from the formation of a second glassy phase of different structure, as suggested by the sample cloudiness. However, from the diffraction pattern alone it is difficult to ascertain whether this second component is a true glass or whether it is

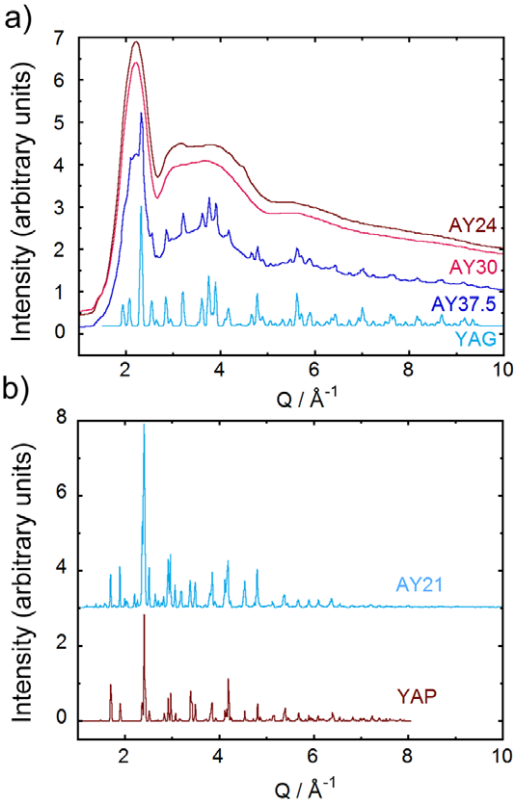

Figure 5. The high-energy x-ray diffraction patterns measured using transmission geometry for several of the $(Y_2O_3)_x(Al_2O_3)_{1-x}$ spheres shown in figure 1. In (a), the diffraction patterns for the $x = 0.24$, 0.30 and 0.375 samples are compared with the powder diffraction pattern for pure crystalline YAG (lowest curve). In (b), the diffraction pattern for the $x = 0.21$ sample is compared with the powder diffraction pattern for pure crystalline YAP (lowest curve). The curves are displaced vertically for clarity of presentation.

an unknown crystalline phase with Bragg peaks that are highly broadened due to particle size effects. The latter hypothesis is consistent with the optical microscopy measurements (figure 2) which show that any inclusions must be of size $\lesssim 1$ μm. An alternative explanation is that the cloudiness arises from spinodal decomposition of the liquid before it passes through the glass transition. Finally, the diffraction pattern for the $x = 0.21$ sample is dominated by the Bragg peaks from YAP. The second phase (or phases) could not be unambiguously identified, although there is evidence for crystalline Al_2O_3 but no evidence for the other intermediate crystalline compounds of the Y_2O_3–Al_2O_3 pseudo-binary system, namely $Y_3Al_5O_{12}$ and $Y_4Al_2O_9$ (Cockayne 1985). The sample composition indicates the formation of a material containing crystalline YAP and Al_2O_3 in the ratio 1:1.38.

4. Discussion

4.1. Equilibrium and metastable phase diagrams for the yttria–alumina system

The phase diagram and crystallization behaviour of the yttria–alumina system has been the subject of considerable study, reflecting the importance of YAG as a host for rare-earth

ions in laser and other optical applications (Yoder and Keith 1951, Cockayne and Lent 1979, Caslavsky and Viechnicki 1980, Cockayne 1985, Gervais *et al* 1997). The equilibrium phase diagram shows the formation of three stable crystalline compounds between the Y_2O_3 and Al_2O_3 end members, namely $Y_3Al_5O_{12}$ (YAG), $YAlO_3$ (YAP) and $Y_4Al_2O_9$, which is sometimes called yttrium aluminium monoclinic (or YAM). The melting point of YAG is reported to be in the range from 1940 °C (Caslavsky and Viechnicki 1980) to 1970 °C (Cockayne 1985). In experiments, the compounds that are actually formed on cooling liquid Y_2O_3–Al_2O_3 mixtures is dependent *inter alia* on the temperature from which the melt is quenched and on the quench rate. For example, moderate supercooling at the YAG ($x = 0.375$) composition favours the formation of crystalline YAP and Al_2O_3, rather than YAG, in the absence of YAG seeding (Cockayne and Lent 1979). The corresponding metastable phase diagram, as reported by Caslavsky and Viechnicki (1980) and Cockayne (1985), shows a supercooled liquid state in the range $0.20 \lesssim x \lesssim 0.45$ which is bounded by a metastable melting curve with a eutectic in the range $0.23 \leqslant x \leqslant 0.28$ and the absence of any stable YAG phase (see figure 6). Faster quench rates, leading to liquids with an increased degree of supercooling, are made accessible by aerodynamic levitation methods. The results obtained for the $x = 0.375$ composition by Gervais *et al* (1997) show that, as the degree of supercooling is increased, the liquid first forms a mixture of crystalline YAP and Al_2O_3, then crystalline YAG and finally a glass (which crystallizes to form YAG on reheating to ≃980 °C). Similar observations were made by Gervais *et al* (1997) for a range of compositions about $x = 0.375$.

4.2. Glass formation for $(Y_2O_3)_x(Al_2O_3)_{1-x}$ with $0.25 \lesssim x \lesssim 0.33$

Aasland and McMillan (1994) investigated the yttria–alumina system, including the glass forming region, by using an iridium wire furnace and optical microscopy. They concluded that, on quenching liquids in the composition range $0.24 \leqslant x \leqslant 0.32$, a second liquid phase spontaneously forms in the supercooled regime, which leads to samples comprising two glassy phases with identical composition but different density. The nucleation temperature of the second liquid phase, T_{l-l}, was observed to be at ≃1220 °C for $x = 0.24$ and at ≃1150 °C for $x = 0.32$, and is represented by the dash–dot–dot curve in figure 6. The glass transition temperature T_g was estimated to be 1150 °C for all of the glass forming compositions and is represented by the dotted curve in figure 6. The lack of sensitivity of T_g to composition is supported by the work of Nagashio and Kuribayashi (2002). Aasland and McMillan (1994) assumed that the locus of crystallization temperatures for the deeply supercooled liquid T_{cryst} (dash–dot curve in figure 6) has the same form as the metastable melting curve. The glass forming region corresponds to the temperature range where $T_g > T_{cryst}$.

The samples produced in the present work by the contactless aerodynamic levitation technique show rather different behaviour. In particular, it was possible to produce only single-phase glasses for the compositions $x = 0.27$ (which is near to the eutectic in the metastable phase diagram of figure 6) and $x = 0.33$, even when the quench rate was reduced by controlled laser cooling. This reduction eventually led to the observation of recalescence and samples having a high degree of crystallinity. The onset of this

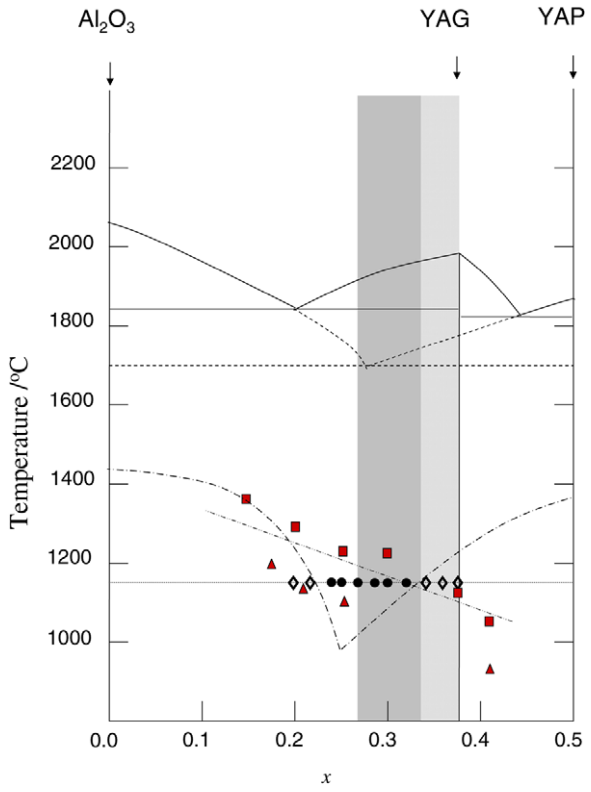

Figure 6. The equilibrium (solid curves) and metastable (dashed curves) phase diagrams for the $(Y_2O_3)_x(Al_2O_3)_{1-x}$ system for $0 \leqslant x \leqslant 0.5$, as adapted from Caslavsky and Viechnicki (1980) and Cockayne (1985). The Al_2O_3, YAG and YAP compositions are indicated. It should be noted that the position of the metastable eutectic at ≃0.27 is slightly different to that indicated by Aasland and McMillan (1994) at ≃0.25 (the mean of the values reported by Caslavsky and Viechnicki (1980) and Cockayne and Lent (1979)). According to Aasland and McMillan (1994), T_g is given by the horizontal dotted line, the solid circles show the two phase glass forming compositions, the open diamonds show the compositions where glass formation does not occur, the v-shaped dash–dot curve gives the crystallization temperature of the deeply supercooled liquid, T_{cryst}, and the dash–dot–dot curve gives the liquid–liquid transition temperature, T_{l-l}, where a second liquid phase was observed to nucleate. Note that T_{cryst} was assumed by Aasland and McMillan (1994) to have the same form as the metastable melting curve, so the position of the metastable eutectic would be shifted to $x \simeq 0.27$, according to the metastable phase diagram of Cockayne (1985). The dark grey region for $0.27 \lesssim x \lesssim 0.33$ and the light grey region for $0.33 \lesssim x \lesssim 0.375$ mark the composition ranges where it was possible, in the present work, to produce either single-phase glasses or glasses containing crystalline YAG inclusions, respectively. The (red) triangles show the crystallization temperatures found in the present work for the samples prepared using a quench rate of ≃300 °C s^{-1} at 1200 °C. The (red) squares show the crystallization temperatures observed in the present work at the lower quench rate of ≃40 °C s^{-1} at 1200 °C which was required in order to crystallize the good glass forming sample at $x = 0.3$.

crystallization process is marked by the (red) squares in figure 6 and occurs very close to the T_{l-l} values reported by Aasland and McMillan (1994). No evidence was therefore found for liquid–liquid phase separation and two-phase glass formation for the composition range $0.27 \lesssim x \lesssim 0.33$. The present results are consistent with the work of Nagashio and Kuribayashi (2002), who studied the $(Y_2O_3)_x(Al_2O_3)_{1-x}$ system over the composition range $0.25 \leqslant x \leqslant 0.375$ by using an aero-acoustic levitation and laser system, another method of *containerless* processing.

4.3. $(Y_2O_3)_x(Al_2O_3)_{1-x}$ samples with $x \gtrsim 0.33$

In the present work we could not produce perfect glassy materials at the YAG ($x = 0.375$) composition. In every case the cooled sphere contained some crystalline YAG inclusions in a glassy matrix. The amount of included crystalline phase increased with decreasing cooling rate, as assessed optically and by the degree of Bragg scattering observed in high-energy, high-resolution x-ray diffraction experiments. Almost completely transparent samples could be formed by using a quench rate of $\simeq$300 °C s^{-1} at 1200 °C, but there remained a small number of virtually invisible inclusions that gave rise to sharp Bragg peaks in the x-ray diffraction patterns. Nagashio and Kuribayashi (2002) also found that, as the composition approaches $x = 0.375$, small spherical inclusions of crystalline YAG precipitated in their samples. However, they did succeed in obtaining single-phase YAG glass by very rapid splat quenching of the levitated liquid between metal anvils. These observations are consistent with the results of Gervais *et al* (1997).

Yttria–alumina glasses, produced by aero-acoustic and aerodynamic levitation, were also studied by Weber and co-workers (Weber *et al* 2000a, 2004) using quench rates comparable to the present work. They reported the existence of spherical inclusions with a similar morphology to those we observed at the YAG composition. However, x-ray diffraction data showed no Bragg scattering and, even though evidence of crystallization was observed in neutron diffraction data, it was concluded that YAG forms a two-phase polyamorphic glass. In later work, however, Johnson and Kriven (2001) made a thorough investigation of YAG crystallization using the same aerodynamic levitation method and, in this case, crystalline YAG inclusions in the as-quenched samples were observed by x-ray diffraction. The reason is unclear for the absence of Bragg peaks in the x-ray diffraction study of Weber *et al* (2004) but the appearance of these peaks in their neutron diffraction study and in the x-ray diffraction study of Johnson and Kriven (2001).

It is interesting to compare the pyrometry traces in figure 3 and relate them to the properties observed for the solid samples. At $x = 0.41$, steady cooling is observed until rapid recalescence occurs at $T \simeq 900$ °C. The steepness of the rise in temperature on recalescence and the subsequent fast decay is consistent with a rapid (almost instantaneous) nucleation of large crystals from the liquid and accounts for the polycrystalline non-spherical shape of the resulting sample (see figure 1). In comparison, for the case of the single-phase glass forming compositions ($0.27 \lesssim x \lesssim 0.33$) there is a fast and continuous decrease in temperature as the sample freely cools, and there is no evidence for a rapid release of latent (excess) heat associated with crystallization. Close inspection of the cooling curve for the cloudy sample at $x = 0.375$ shows that some excess heat is evolved compared to the single-phase glass forming composition $x = 0.33$, as manifested by a longer decay time for the temperature in the range between 1300 and 800 °C (see figure 3). The absence of a sharp recalescence feature but slow evolution of excess heat is consistent with an independent and slow nucleation of small crystalline inclusions which lead to the Bragg peaks observed in figure 5. As shown in figure 4, slower cooling of the $x = 0.375$ composition under controlled conditions ($\simeq$100 °C s^{-1} at 1200 °C) leads to a sharp recalescence feature akin to the $x = 0.41$ composition.

The degree of supercooling exhibited by liquids having the YAG composition highlights the difficulty associated with homogeneous nucleation and growth of the crystalline YAG phase. The aerodynamic levitation experiments of Gervais *et al* (1997) show that, as the degree of supercooling is increased, the liquid first forms a mixture of crystalline YAP and Al_2O_3, then crystalline YAG and finally a glass. This problem in forming nucleation centres with a critical size required for growth is related, in part, to the large unit cell of YAG (Prince 1957, Cockayne and Lent 1979, Cockayne 1985) which contains 160 atoms in which 60% of the Al atoms are tetrahedrally coordinated and 40% of the Al atoms are octahedrally coordinated to oxygen atoms, giving a mean Al–O coordination number of 4.8. By comparison, YAP (Ross *et al* 2004) and the thermodynamically stable corundum structure of α-Al_2O_3 (Levin and Brandon 1998) have small unit cells, containing 20 and 30 atoms respectively, in which all of the Al is octahedrally coordinated by oxygen atoms. γ-Al_2O_3 (average of $53\frac{1}{3}$ atoms in the unit cell) and other alumina polymorphs contain both octahedral and tetrahedral sites, leading to an average Al–O coordination number between 4 and 6 (Levin and Brandon 1998). On the other hand, x-ray diffraction experiments on the supercooled liquid phase show that aluminium has a predominantly tetrahedral coordination environment, although deeply supercooled liquids levitated on argon gas show a mean Al–O coordination number of $\simeq$5 (Weber *et al* 2000b), while ^{27}Al nuclear magnetic resonance experiments on the liquid at 1970 °C place the fraction of AlO_4 tetrahedra at 80%, with both AlO_5 and AlO_6 making up the remaining species (Coutures *et al* 1990). Gervais *et al* (1997) explain the observed behaviour of liquid YAG as resulting from a competition between, firstly, the need for high Al and Y diffusion coefficients if phase separation into YAP and Al_2O_3 is to occur and, secondly, the comparatively large nucleation embryos needed to form YAG. At higher temperatures (fast diffusion) the former wins, whereas at lower temperatures the latter wins. This competition also explains the propensity for YAG to form a partial glassy phase on rapid cooling, as neither process can take place fast enough to prevent glass formation. It should be noted that the viscosity of liquid YAG shows typical fragile behaviour, e.g. it varies rapidly with temperature in the supercooled regime near T_g (Weber *et al* 1998).

4.4. $(Y_2O_3)_x(Al_2O_3)_{1-x}$ samples with $x \lesssim 0.24$

In the present work, the character of the cloudy samples at the $x = 0.24$ composition is substantially different to that seen for compositions approaching YAG. For example, the optical images of figure 2 show that any inclusions are sub-micron in size and the x-ray diffraction pattern of figure 5 shows no obvious Bragg peaks. However, it is not possible to use this diffraction pattern to establish unambiguously whether the observed additional structure is due to (i) a second glassy phase of different density but the same composition that arises from liquid–liquid phase separation, (ii) a second glassy phase of different composition that arises from spinodal decomposition, or (iii) a large number of sub-micron nano-crystals which give Bragg peaks with considerable particle size broadening. All of these scenarios could lead to the distinct sample cloudiness that we observe at this composition.

As the composition is reduced from $x = 0.24$ to 0.20, the ability to form bulk glassy samples becomes increasingly difficult (Aasland and McMillan 1994, Wilding *et al* 2005) and, for the levitation system used in the present work, crystallization always takes place at $x = 0.21$ for a sample size of ∼2.3–2.5 mm diameter. The corresponding x-ray diffraction data, which are shown in figure 5, indicate the formation of a multiphase crystalline material comprising YAP but not YAG. This observation is consistent with the metastable phase diagram of figure 6, which shows a eutectic at $x \simeq 0.27$ with Al_2O_3 and YAP endpoints.

Again, it is interesting to compare the pyrometry traces in figure 3 and relate them to the properties observed for the solid samples. Close inspection of the cooling curve for the cloudy $x = 0.24$ sample shows that some excess heat is evolved, compared to the single-phase glass forming compositions, which is manifested by a longer decay time for the temperature in the range between 1300 and 800 °C. However, the x-ray diffraction data of figure 5 do not enable a clear distinction to be made between the scenarios where there is (i) a slow nucleation and growth of small crystalline inclusions or (ii) the formation of a second liquid or glassy phase. By comparison, at the $x = 0.21$ composition a strong recalescence phenomenon is observed, but its character is very different from that seen for $x = 0.41$. Instead, the rise in temperature takes place over a period of ≃0.5 s and there is a steady evolution of excess heat for ≃1.5 s before the sample resumes black-body cooling. As shown in figure 4, this general behaviour is repeated if a sample is cooled more slowly under controlled conditions. When the quench rate of the $x = 0.24$ sample is reduced, the appearance of the cooling curve is similar to that for $x = 0.21$. The nucleation and growth time for YAP and Al_2O_3 is therefore much longer than the corresponding time for YAG near the $x = 0.375$ composition. For the YAG composition, Gervais *et al* (1997) observed the formation of YAP and alumina under slow quench conditions but the recalescence feature remained sharp.

4.5. Does polyamorphism exist for the $(Y_2O_3)_x(Al_2O_3)_{1-x}$ system?

For the composition range $0.25 \lesssim x \lesssim 0.33$ there are clear distinctions to be made between the results presented by Aasland and McMillan (1994) and those presented in the present work and by Nagashio and Kuribayashi (2002). In the former case, two phase glasses were formed at all of the compositions and the use of an iridium wire furnace leads to the possibility of inhomogeneous nucleation caused by the melt interacting with the container walls (Aasland and McMillan 1994). In the latter case, however, the use of levitation methods leads to a suppression of heterogeneous nucleation and a region of homogeneous single-phase glass formation was found. The liquid–liquid phase transition line reported by Aasland and McMillan (1994) occurs at temperatures that are comparable to those found in this work for the onset of crystallization (see figure 6). The existence and mechanism for the occurrence of a liquid–liquid phase transition for the composition range $0.25 \lesssim x \lesssim 0.33$ is therefore debatable. For instance, at what stage would a second phase stop being classified as a glass that has formed from a dynamically arrested metastable liquid–liquid phase transition and start being classified as an embryonic crystal?

In the more recent work of McMillan and co-workers (Wilding and McMillan 2001, Wilding *et al* 2002a, 2002b, McMillan *et al* 2003, Wilson and McMillan 2004, McMillan *et al* 2007) it is reported that large (micron-sized) regions of isolated HDA (high-density) and LDA (low-density) polyamorphs can be produced by quenching appropriate Y_2O_3–Al_2O_3 liquids. In a revised sample procedure, the tip of a rod of the chosen composition produced by sol–gel methods is heated in an image furnace so that a liquid droplet, in contact with the solid, is allowed to form. On further heating, this droplet detaches from the rod, whereupon it is allowed to fall through a platinum grid (to reduce particle size) and then quenched into water. By comparison with the LDA phase, the HDA phase is reported to have a mass density that is 4% higher and a glass transition temperature T_g that is lower. The favoured composition range for these two-phase glasses is now given as $0.20 \leqslant x \leqslant 0.24$ and not at the higher yttria contents of the original work. It is also claimed (McMillan *et al* 2003) that similar materials can be produced by roller quenching, although the precise methods are not stated.

Although we have not been able to produce samples containing such clearly isolated regions by using levitation methods, the revised composition range for the formation of two-phase glasses is not inconsistent with the observations that we have made for compositions close to $x = 0.24$, as manifested by the cloudiness of the samples (see figure 1) and the additional structure observed in the x-ray diffraction pattern compared to $x = 0.30$ (see figure 5). Nevertheless, the discrepancies between the results suggest that, in the non-levitation procedures, different processes take place such as heterogeneous nucleation from centres that remain in the liquid as it detaches from the solid rod or which form as the liquid makes contact with the platinum grid or quenching rollers.

It is notable that the cloudy $x = 0.24$ sample shown in figure 1 also has a large hole in its interior. Similar holes were not observed in any of the homogeneous single-phase glasses produced in the present work, but they were observed in cloudy samples made by Weber *et al* (2000a) using levitation methods. The holes are attributed to sample shrinkage on cooling and

suggest that regions of the liquid are subjected to considerable tension (negative pressure) as a precursor to void formation. As a result, the interior of the liquid will become mechanically unstable, due to the significant internal pressure gradients that accompany differential rates of cooling and solidification, and it is possible that these instabilities lead to different regions which favour the formation of HDA and LDA material as the supercooled liquid solidifies. It is therefore plausible that the stability limit (Speedy 1982), percolation and liquid–liquid phase transition hypotheses, outlined by Mishima and Stanley (1998) in relation to the formation of HDA and LDA water, have relevance to the formation of glasses in the Y_2O_3–Al_2O_3 system. It could also be surmised that similar tension in the liquid, on dropping through a platinum grid or onto quenching rollers, could also be present when forming the HDA and LDA material observed by McMillan *et al* (2007).

The $(Y_2O_3)_x(Al_2O_3)_{1-x}$ system clearly merits further investigation in order to elucidate the precise conditions (temperature, pressure, quench rate) that promote the formation of two-phase glasses. In this context it is interesting to note that the neutron and x-ray diffraction work of Wilding and co-workers (Wilding *et al* 2002a, 2005) show that the structure of glasses formed for both the $x = 0.25$ and 0.20 compositions is dominated by tetrahedral AlO_4 conformations, although the diffraction patterns for $x = 0.20$ showed Bragg peaks that were attributed to partial crystallization of the LDA phase. Analysis of our diffraction data (which is limited by the available Q-range of $1.35 \leqslant Q \leqslant 23$ Å^{-1}) gives an Al–O coordination number of 4.1 ± 0.2 for $0.24 \leqslant x \leqslant 0.375$ and confirms this tendency for tetrahedral coordination in the glass. Also, the $x = 0.25$ composition corresponds to an Al:O ratio of 1:2, which enables the possibility of forming a continuous random network of corner-shared AlO_4 tetrahedra, should the aluminium be exclusively four-fold coordinated by oxygen atoms. To explore the $0.24 \leqslant x \leqslant 0.27$ composition range further, we have carefully fabricated a series of samples with x increasing in 0.005 steps by using the levitation method described in this paper. It was found that the samples formed for $x < 0.25$ were always cloudy and similar in form to the $x = 0.24$ sample shown in figure 1. In contrast, it was possible to make clear glassy samples for all compositions with $x \geqslant 0.255$. For $x = 0.25$, the samples sometimes appeared clear and sometimes cloudy, a variation that could be explained by the difficulty of obtaining precise sample compositions and quenching conditions. Hence, single-phase glass formation appears to occur for $x \gtrsim 0.25$, where a network of corner-shared AlO_4 tetrahedra can be maintained, provided that these structural motifs contain non-bridging oxygen atoms. However, for compositions of $x \lesssim 0.25$, where cloudy samples always form, the maintenance of a tetrahedral network requires an oxygen coordination number greater than two or edge-sharing conformations. Questions that need to be addressed with regard to glass formation in this system therefore include the composition dependence of the aluminium and yttrium coordination environments and the diffusion coefficients of these species in both the liquid, supercooled liquid and glassy states, especially in the region around $x = 0.25$.

5. Conclusions

We have undertaken a study of glass formation from aerodynamically levitated liquids in the $(Y_2O_3)_x(Al_2O_3)_{1-x}$ system by using pyrometric, optical imaging and x-ray diffraction methods. The optimum glass formation region occurs for the composition range $0.25 \lesssim x \lesssim 0.33$. At the extremes of this range the materials show an increasing tendency to phase separate. For the Y_2O_3-rich compositions ($0.33 \lesssim x \leqslant 0.375$), we conclude that there is a glassy matrix in which small ($\lesssim$40 μm) crystallites of yttrium aluminium garnet (YAG) nucleate. With very rapid quenching methods it is possible to produce a single-phase glass at the YAG ($x = 0.375$) composition (Nagashio and Kuribayashi 2002). For compositions just less than $x = 0.25$, the nucleation processes taking place in the liquid appear to be slow and complex and give rise to microscopic density or compositional fluctuations that cause cloudiness. In order to resolve some of the discrepancies observed in the properties of liquid, supercooled liquid and glassy $(Y_2O_3)_x(Al_2O_3)_{1-x}$, a further systematic and detailed study of the structure and dynamics of this system is required, especially around the $x = 0.25$ composition.

Acknowledgments

We would like to thank Martin Wilding for helpful discussions during the preparation of this manuscript and Jeff Odell for assistance in using the phase contrast microscope. Lawrie Skinner thanks the UK Engineering and Physical Sciences Research Council (EPSRC) for the award of a Doctoral Training Award. We would also like to acknowledge use of the EPSRC Chemical Database Service at Daresbury.

References

Aasland S and McMillan P F 1994 *Nature* **369** 633
Caslavsky J L and Viechnicki D J 1980 *J. Mater. Sci.* **15** 1709
Cockayne B 1985 *J. Less-Common Met.* **114** 199
Cockayne B and Lent B 1979 *J. Cryst. Growth* **46** 371
Coutures J P, Massiot D, Bessada C, Echegut P, Rifflet J C and Taulelle F 1990 *C. R. Acad. Sci. Paris* **310** 1041
Euler F and Bruce J A 1965 *Acta Crystallogr.* **19** 971
Fischer H E, Barnes A C and Salmon P S 2006 *Rep. Prog. Phys.* **69** 233
Fletcher D A, McMeeking R F and Parkin D 1996 *J. Chem. Inf. Comput. Sci.* **36** 746
Gervais M, Le Floch S, Gautier N, Massiot D and Coutures J P 1997 *Mater. Sci. Eng.* B **45** 108
Gervais M, Le Floch S, Rifflet J C, Coutures J and Coutures J P 1992 *J. Am. Ceram. Soc.* **75** 3166
Johnson B R and Kriven W M 2001 *J. Mater. Res.* **16** 1795
Levin I and Brandon D 1998 *J. Am. Ceram. Soc.* **81** 1995
McMillan P F, Wilson M and Wilding M C 2003 *J. Phys.: Condens. Matter* **15** 6105
McMillan P F, Wilson M, Wilding M C, Daisenberger D, Mezouar M and Greaves G N 2007 *J. Phys.: Condens. Matter* **19** 415101
Mishima O and Stanley H E 1998 *Nature* **396** 329
Morse H W and Donnay J D H 1932 *Am. J. Sci.* **23** 440
Morse H W and Donnay J D H 1936 *Am. Mineral.* **21** 391

Nagashio K and Kuribayashi K 2002 *J. Am. Ceram. Soc.* **85** 2353
Nordine P C, Weber J K R and Abadie J G 2000 *Pure Appl. Chem.* **72** 2127
Prince E 1957 *Acta Crystallogr.* **10** 787
Ross N L, Zhao J and Angel R J 2004 *J. Solid State Chem.* **177** 1276
Speedy R J 1982 *J. Phys. Chem.* **86** 982
Weber J K R, Abadie J G, Hixson A D, Nordine P C and Jerman G A 2000a *J. Am. Ceram. Soc.* **83** 1868
Weber J K R, Benmore C J, Siewenie J, Urquidi J and Key T S 2004 *Phys. Chem. Chem. Phys.* **6** 2480
Weber J K R, Felten J J, Cho B and Nordine P C 1998 *Nature* **393** 769
Weber J K R, Krishnan S, Ansell S, Hixson A D and Nordine P C 2000b *Phys. Rev. Lett.* **84** 3622
Wilding M C, Benmore C J and McMillan P F 2002a *J. Non-Cryst. Solids* **297** 143
Wilding M C and McMillan P F 2001 *J. Non-Cryst. Solids* **293–295** 357
Wilding M C, McMillan P F and Navrotsky A 2002b *Physica* A **314** 379
Wilding M C, Wilson M and McMillan P F 2005 *Phil. Trans. R. Soc.* A **363** 589
Wilson M and McMillan P F 2004 *Phys. Rev.* B **69** 054206
Yoder H S and Keith M L 1951 *Am. Mineral.* **36** 519